

The Birth of a Relativistic Outflow in the Unusual γ -ray Transient Swift J164449.3+573451

B. A. Zauderer¹, E. Berger¹, A. M. Soderberg¹, A. Loeb¹, R. Narayan¹, D. A. Frail², G. R. Petitpas¹, A. Brunthaler³, R. Chornock¹, J. M. Carpenter⁴, G. G. Pooley⁵, K. Mooley⁴, S. R. Kulkarni⁴, R. Margutti⁶, D. B. Fox⁷, E. Nakar⁸, N. A. Patel¹, N. H. Volgenau⁹, T. L. Culverhouse⁹, M. F. Bietenholz^{10,11}, M. P. Rupen², W. Max-Moerbeck⁴, A. C. S. Readhead⁴, J. Richards⁴, M. Shepherd⁴, S. Storm¹², & C. L. H. Hull¹³

¹ Harvard-Smithsonian Center for Astrophysics, 60 Garden St., Cambridge, MA 02138, USA

² National Radio Astronomy Observatory, P.O. Box 0, Socorro, NM 87801, USA

³ Max-Planck-Institut für Radioastronomie, Auf dem Hügel 69, 53121 Bonn, Germany

⁴ Department of Astronomy, California Institute of Technology, Pasadena, CA 91125, USA

⁵ Mullard Radio Observatory, Cavendish Laboratory, Cambridge UK

⁶ INAF Osservatorio Astronomico di Brera, via Bianchi 46, Merate 23807, Italy

⁷ Department of Astronomy, Pennsylvania State University, University Park, PA 16802, USA

⁸ School of Physics & Astronomy, Tel Aviv University, Tel Aviv 69978, Israel

⁹ California Institute of Technology, Owens Valley Radio Observatory, Big Pine, CA 93513, USA

¹⁰ Hartebeesthoek Radio Astronomy Observatory, PO Box 443, Krugersdorp, 1740 South Africa

¹¹ Department of Physics and Astronomy, York University, Toronto, Ontario, Canada

¹² Department of Astronomy, University of Maryland, College Park, MD 20742

¹³ Radio Astronomy Laboratory, University of California, Berkeley, CA 94720

Active galactic nuclei (AGN), powered by long-term accretion onto central supermassive black holes, produce¹ relativistic jets with lifetimes of $> 10^6$ yr that preclude observations at birth. Transient accretion onto a supermassive black hole, for example through the tidal disruption^{2,3} of a stray star, may therefore offer a unique opportunity to observe and study the birth of a relativistic jet. On 2011 March 25, the *Swift* γ -ray satellite discovered⁴ an unusual transient source (Swift J164449.3+573451) potentially representing^{5,6} such an event. Here we present the discovery of a luminous radio transient associated with Swift J164449.3+573451, and an extensive set of observations spanning centimeter to millimeter wavelengths and covering the first month of evolution. These observations lead to a positional coincidence⁷ with the nucleus of an inactive galaxy, and provide direct evidence for a newly-formed relativistic outflow, launched by transient accretion onto a $10^6 M_{\odot}$ black hole. While a relativistic outflow was not predicted in this scenario, we show that the tidal disruption of a star naturally explains the high-energy properties, radio luminosity, and the inferred rate of such events. The weaker beaming in the radio compared to γ -rays/X-rays, suggests that radio searches may uncover similar events out to redshifts of $z \sim 6$.

This paper has been submitted to Nature. You are free to use the results here for the purpose of your research. In accordance with the editorial policy of Nature, we request that you not discuss this result in the press. If you have any question or need clarifications please contact Ashley Zauderer (bzauderer@cfa.harvard.edu) or Edo Berger (eberger@cfa.harvard.edu).

Upon the discovery⁴ of Swift J164449.3+573451, and the identification of a galaxy at a redshift⁶ of $z = 0.354$ within the *Swift* X-ray localization region (1.4'' radius), we initiated radio observations of the transient on 2011 March 29.36 UT with the Expanded Very Large Array (EVLA) at a frequency of 5.8 GHz and discovered an unresolved source with a flux density of $31 \pm 7 \mu\text{Jy}$. Astrometric matching demonstrated that the radio source coincides with the galaxy nucleus (Figure 1), subsequently confirmed⁶ with other data. A follow-up EVLA observation 0.9 d later revealed that the source brightened to $53 \pm 10 \mu\text{Jy}$, thereby conclusively linking the X-ray/ γ -ray transient and the galaxy for the first time. The galaxy exhibits no evidence⁶ for an active nucleus (see Figure 1 in online Supplementary Information; SI), and the lack of previous γ -ray/X-ray activity argues⁴ against an AGN flare origin.

We carried out additional observations at multiple frequencies spanning 1–345 GHz with several cm- and mm-wave facilities (see SI Table 1). The spectral energy distribution (SED) in this frequency range on 2011 March 30 UT ($\Delta t \sim 5$ d) is well described by a power law with $F_\nu \propto \nu^{1.3 \pm 0.1}$ up to $F_\nu(345 \text{ GHz}) = 35 \pm 1 \text{ mJy}$. The steep power law requires self-absorbed synchrotron emission. The weak near-infrared (NIR) variability⁶ indicates $F_\nu(2.5 \mu\text{m}) \lesssim 0.1 \text{ mJy}$, while the lack of optical variability leads⁶ to an upper bound of $F_\nu(0.64 \mu\text{m}) < 2 \mu\text{Jy}$. The SED therefore peaks in the millimeter band, with a best-fit rest-frame peak frequency and flux density of $\nu_p \sim 6 \times 10^{11} \text{ Hz}$ and $F_{\nu,p} \sim 80 \text{ mJy}$, respectively (Figure 2). The non-detection of optical variability requires significant rest-frame extinction of $A_V > 3$ mag, further supporting a nuclear origin. Subsequent SEDs at $\Delta t \sim 10, 15,$ and 22 d exhibit significant evolution, with $\nu_p \propto t^{-1.3}$ and $F_{\nu,p} \propto t^{-0.8}$ (Figure 2).

For synchrotron sources there is a well-defined minimum energy, achieved⁸ near equipartition between the fractional energies in the relativistic electrons (ϵ_e) and magnetic fields (ϵ_B). This condition defines⁹ the equipartition radius: $\theta_{\text{eq}} = 110 d_{\text{L,Mpc}}^{-1/19} F_{\nu,p,\text{mJy}}^{9/19} \nu_{p,\text{GHz}}^{-1} \mu\text{as}$. From the March 30 UT SED we find $\theta_{\text{eq}} \sim 1 \mu\text{as}$ ($r_{\text{eq}} \sim 1.5 \times 10^{16} \text{ cm}$) and hence mildly relativistic expansion with a Lorentz factor of $\Gamma \sim 2$. A more detailed model that accounts¹⁰ for relativistic effects leads to a similar

result, $r_{\text{eq}} \sim 1 \times 10^{16}$ cm and $\Gamma \sim 1.2$ (see SI). From the observed SED temporal evolution we find that the source continues to expand relativistically with nearly constant velocity (see SI text). Extrapolating the linear trend in radius we find a formation epoch in the range 2011 March 23-26 UT, in excellent agreement with the initial γ -ray detection on 2011 March 25 UT (see SI Figure 2). This provides independent evidence for a newly-formed relativistic outflow.

An angular size of a few μas will inevitably lead to variability in the low frequency radio emission due to interstellar scintillation, with the amplitude of modulation depending¹¹ on the ratio of the source size (θ_s) to the Fresnel scale (θ_F). For the line of sight to Swift J164449.3+573451 the maximum modulation ($m_p \sim 1$) is expected¹² at $\nu_0 \sim 10$ GHz, for $\theta_s \sim \theta_F \sim 1 \mu\text{as}$. The observed modulation inferred from our detailed radio light curves is tens of percent at 5–7 GHz and a few percent at 15 GHz (Figure 3), leading to a projected radius of $\theta_s \sim 5 \mu\text{as}$, or $\Gamma \sim 5$. This provides independent evidence for a relativistic outflow. Our radio observations with Very Long Baseline Interferometry (VLBI) at a frequency of 22 GHz place an upper bound on the size of $r < 0.8$ pc, consistent with the synchrotron and scintillation analyses, and providing an upper bound on the lifetime of the event of < 1.7 yr for an expansion with $\Gamma \sim 2$ (see SI text).

The mean X-ray luminosity during the four radio epochs exceeds the synchrotron peak by a factor of $\sim 10^3$ and therefore requires a distinct origin (Figure 2). One potential mechanism to generate the large X-ray luminosity is inverse Compton (IC) scattering of radio synchrotron photons by the relativistic electrons (synchrotron self-Compton: SSC), but from the relativistic model we find a predicted SSC X-ray luminosity of only $\sim 2 \times 10^{45}$ erg s⁻¹ (see SI). Similarly, although order of magnitude variations in brightness are seen in the X-rays, our detailed radio light curves do not reveal coincident variations as would be expected for SSC (Figure 3). We therefore conclude that the X-ray emission is dominated by a distinct, and more compact emission region, most likely at the base of the outflow.

Having established the birth of a relativistic outflow, coincident with the nucleus of the host galaxy, we briefly describe a model to power the outflow through transient accretion⁵ onto a supermassive black hole (SMBH). The host galaxy luminosity, $M_B \sim 18.2$ mag, implies¹³ a modest SMBH mass of $\sim 10^5$ – $10^6 M_\odot$. The duration of the bright early phase in the X-ray light curve, $\sim 10^5$ s, coincides with the debris fallback time for a solar-mass star tidally disrupted at a pericenter distance $R_p \sim 13(M_{\text{SMBH}}/10^6 M_\odot)^{-5/6}$ Schwarzschild radii. The most bound stellar debris is expected to feed the black hole at an initial rate of¹⁴ $(\frac{1}{2}M_\odot)/10^5$. With a radiative efficiency of $> 1\%$ at R_p , this can account for the

observed X-ray luminosity. However, this luminosity is $\sim 10^3$ times the Eddington limit for a $10^6 M_\odot$ black hole, leading inevitably to a highly collimated outflow, the origin of the radio-emitting relativistic outflow found here.

We conclude with several key implications of our results. First, our initial estimate of the energy, $E_K \sim 3 \times 10^{50}$ erg at $\Delta t \sim 22$ d (see SI Table 2), corresponds to the Eddington luminosity of a $10^6 M_\odot$ black hole, lending support to the tidal disruption scenario, and suggesting that the X-ray/ γ -ray emission is collimated by a factor of $\sim 10^3$. Long-term radio monitoring will test this result by providing precise beaming-independent calorimetry^{15,16} of the true energy release. Continued radio observations will also uniquely probe the density structure near a previously-dormant supermassive black hole as the ambient medium is swept up by the relativistic outflow. From the existing data we find $n_e \propto r^{-2.4}$ (see SI). Second, with continued expansion we expect that VLBA observations will resolve the radio source on a timescale of ~ 2 yr, and directly confirm the relativistic expansion; from the observed flux density evolution we predict a peak of a few mJy at several GHz on this timescale, within the reach of the VLBA. Third, from the detection of a single such event in 6 years of *Swift* operations we infer a rate of $\sim 0.1 \text{ Gpc}^{-3} \text{ yr}^{-1}$, much lower than the predicted¹⁷ tidal disruption rate of $10^2 - 10^3 \text{ Gpc}^{-3} \text{ yr}^{-1}$, or upper limits from current radio surveys¹⁸ of $< 10^3 \text{ Gpc}^{-3} \text{ yr}^{-1}$. This suggests that the properties of Swift J164449.3+573451 are exceedingly rare; if due to jet collimation, the implied beaming fraction is $\sim 10^3$, consistent with the ratio of the observed X-ray luminosity to the Eddington limit and the radio-inferred energy. Finally, past searches^{19–21} for tidal disruption events have focused on the expected¹⁴ bright optical/UV and soft X-ray emission, but the large optical extinction and associated soft X-ray absorption in Swift J164449.3+573451 suggest that radio observations may provide a cleaner signature. This is particularly true if the X-ray/ γ -ray emission is beamed by a factor of $\sim 10^3$. With the EVLA and the Atacama Large Millimeter Array, similar events are detectable to $z \sim 6$.

1. Begelman, M. C., Blandford, R. D. & Rees, M. J. Theory of extragalactic radio sources. *Reviews of Modern Physics* **56**, 255–351 (1984).
2. Hills, J. G. Possible power source of Seyfert galaxies and QSOs. *Nature* **254**, 295–298 (1975).
3. Rees, M. J. Tidal disruption of stars by black holes of 10 to the 6th–10 to the 8th solar masses in nearby galaxies. *Nature* **333**, 523–528 (1988).
4. Burrows, D. N. *et al.* Discovery of the Onset of Rapid Accretion by a Dormant Massive Black Hole. *Submitted to Nature*.
5. Bloom, J. S., Giannios, D., Metzger, B. D., Cenko, S. B., Perley, D. A. *et al.* A relativistic jetted outburst from a massive black hole fed by a tidally disrupted star. *ArXiv:1104.3257*, (2011).
6. Levan, A. J., Tanvir, N. R., Cenko, S. B., Perley, D. A., Wiersema, K. *et al.* An extremely luminous panchromatic outburst from the nucleus of a distant galaxy. *ArXiv:1104.3356*, (2011).
7. Berger, E., Levan, A., Tanvir, N. R., Zauderer, A., Soderberg, A. M. *et al.* GRB 110328A / Swift J164449.3+573451: Radio-optical/NIR astrometry. *GRB Coordinates Network, Circular Service* **1854**, 1 (2011).
8. Readhead, A. C. S. Equipartition brightness temperature and the inverse Compton catastrophe. *Astrophys. J.* **426**, 51–59 (1994).
9. Chevalier, R. A. Synchrotron Self-Absorption in Radio Supernovae. *Astrophys. J.* **499**, 810–819 (1998).
10. Kumar, P. & Narayan, R. GRB 080319B: evidence for relativistic turbulence, not internal shocks. *Mon. Not. R. Astr. Soc.* **395**, 472–489 (2009).
11. Goodman, J. & Narayan, R. Fitting Formula for Flux Scintillation of Compact Radio Sources. *Astrophys. J.* **636**, 510–527 (2006).
12. Cordes, J. M. & Lazio, T. J. W. NE2001.I. A New Model for the Galactic Distribution of Free Electrons and its Fluctuations. *ArXiv:0207156*, (2002).
13. Greene, J. E. & Ho, L. C. A New Sample of Low-Mass Black Holes in Active Galaxies. *Astrophys. J.* **670**, 92–104 (2007).
14. Strubbe, L. E. & Quataert, E. Optical flares from the tidal disruption of stars by massive black holes. *Mon. Not. R. Astr. Soc.* **400**, 2070–2084 (2009).

15. Frail, D. A., Waxman, E. & Kulkarni, S. R. A 450 Day Light Curve of the Radio Afterglow of GRB 970508: Fireball Calorimetry. *Astrophys. J.* **537**, 191–204 (2000).
 16. Shivvers, I. & Berger, E. A Beaming-Independent Estimate of the Energy Distribution of Long Gamma-Ray Bursts: Initial Results and Future Prospects. *Astrophys. J. in press*, 2011.
 17. Wang, J. & Merritt, D. Revised Rates of Stellar Disruption in Galactic Nuclei. *Astrophys. J.* **600**, 149–161 (2004).
 18. Bower, G. C. Constraining the Rate of Relativistic Jets from Tidal Disruptions Using Radio Surveys. *Astrophys. J.* **732**, L12–L15 (2011).
 19. Komossa, S. & Bade, N. The giant X-ray outbursts in NGC 5905 and IC 3599:() hfill Follow-up observations and outburst scenarios. *Astr. Astrophys.* **343**, 775–787 (1999).
 20. Gezari, S., Basa, S., Martin, D. C., Bazin, G., Forster, K. *et al.* UV/Optical Detections of Candidate Tidal Disruption Events by GALEX and CFHTLS. *Astrophys. J.* **676**, 944–969 (2008).
 21. Cenko, S. B., Bloom, J. S., Kulkarni, S. R., Strubbe, L. E., Miller, A. A. *et al.* PTF10iya: A short-lived, luminous flare from the nuclear region of a star-forming galaxy. *ArXiv:1103.0779*, (2011).
-

Acknowledgements E.B. is supported in part by funds from NASA. A. L. is supported in part by NSF and NASA grants. R.M. acknowledges support from a Swift ASI grant and from the Ministry of University and Research of Italy. E.N. is partially supported by IRG and ISF grants. The EVLA and VLBA are operated by the NRAO, a facility of the NSF operated under cooperative agreement by AUI. The SMA is a joint project between the SAO and the ASIAA, and is funded by the Smithsonian Institution and the Academia Sinica. CARMA development and operations are supported by the NSF under a cooperative agreement, and by the Associates of the California Institute of Technology, the University of Chicago, and the states of California, Illinois, and Maryland. The AMI arrays are supported by the University of Cambridge and the STFC. This work is partially based on observations with the 100-m telescope of the MPIfR at Effelsberg. This work made use of data supplied by the UK Swift Science Data Centre at the University of Leicester.

Author Contributions A.Z. and E.B. designed and coordinated the radio observations and analysis among all instruments reported here. A.Z. and D.A.F. performed EVLA observations, data reduction and analysis. G.R.P. observed the source with the SMA, and along with N.A.P. reduced and analyzed the SMA observations. CARMA observations were set up, reduced and analyzed by A.Z., J.M.C. and S.R.K. S.S. and C.L.H.H. obtained the first CARMA observations. N.H.V. and T.L.C. facilitated quick response CARMA observations. R.C. implemented and analyzed MMT and Gemini optical observations. K.M. performed observations with the OVRO 40-m and analyzed results, with advice from S.R.K., A.C.S.R., J.R., M.S., and W.M. G.G.P. performed observations with the AMI Large Array and analyzed the results. A.M.S., A.B., M.F.B. and M.P.R. planned observations with the VLBA and Effelsberg. A.B. reduced the VLBI data. R.M. analyzed and modeled the X-ray data. A.L., R.N. and E.N. provided the theoretical model for a tidal disruption event. The paper was synthesized by A.Z. and E.B. with the primary text written by E.B. and portions of the SI written by E.B., A.Z., R.C., K.M. and A.B. D.B.F. provided feedback on the manuscript. All authors discussed the results and commented on the manuscript.

Author Information Correspondence and requests for materials should be addressed to A.Z. (bzauderer@cfa.harvard.edu) or E.B. (eberger@cfa.harvard.edu).

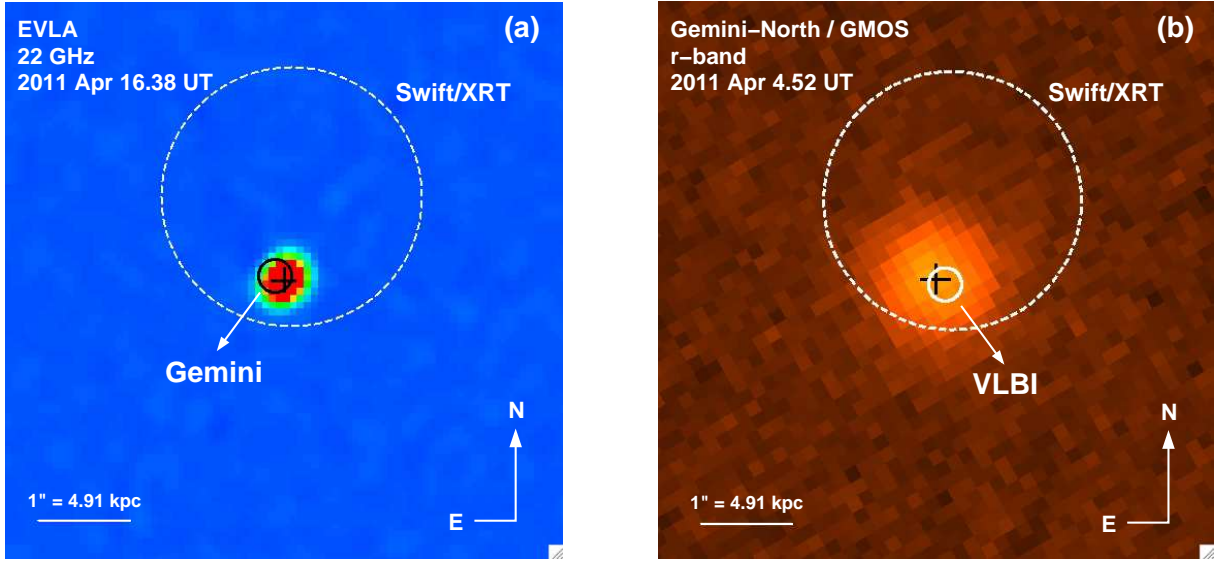


Figure 1. Radio and optical images of Swift J164449.3+573451 and its host galaxy reveal a positional alignment between the transient and the center of the galaxy. (a) The radio image is from the EVLA at a frequency of 22 GHz. The most precise radio position, from VLBI is $\alpha_{J2000} = 16^{\text{h}}44^{\text{m}}49.93130^{\text{s}}$, $\delta_{J2000} = +57^{\circ}34'59.6893'' \lesssim 0.1 \text{ mas}$; see SI). (b) The optical r -band image was obtained on 2011 April 4.52 UT with the Gemini-North 8-m telescope, and has been astrometrically aligned to the Two Micron All Sky Survey (2MASS) catalog using 14 common objects with a resulting root-mean-square uncertainty of 0.13 arcsec in each coordinate (68% confidence level). The galaxy optical centroid is located at $\alpha_{J2000} = 16^{\text{h}}44^{\text{m}}49.942^{\text{s}}$, $\delta_{J2000} = +57^{\circ}34'59.74'' \lesssim 0.01 \text{ arcsec}$. The *Swift*/XRT error circle (large white circle), with a radius of 1.4 arcsec (90% confidence level), contains the galaxy, but cannot be used to locate the X-ray transient position within it. On the other hand, the radio position relative to the astrometric solution of the Gemini image has an uncertainty of only 0.18 arcsec (68% confidence level; this uncertainty is dominated by the astrometric match of the optical image to the 2MASS catalog, not by the radio position itself) and leads to an offset of $0.11 \lesssim 0.18 \text{ arcsec}$, corresponding to a physical scale of $0.5 \lesssim 0.9 \text{ kpc}$ at $z = 0.354$. The radio transient position is therefore consistent with an origin in the nucleus of the host galaxy. (a) The radio centroid is marked by cross-hairs, while the galaxy optical centroid (with an uncertainty of 0.18 arcsec due to 2MASS astrometric solution) is marked by the small black circle. (b) The galaxy optical centroid is marked by cross-hairs, while the radio position (with an uncertainty of 0.18 arcsec due to 2MASS astrometric solution) is marked by the small white circle.

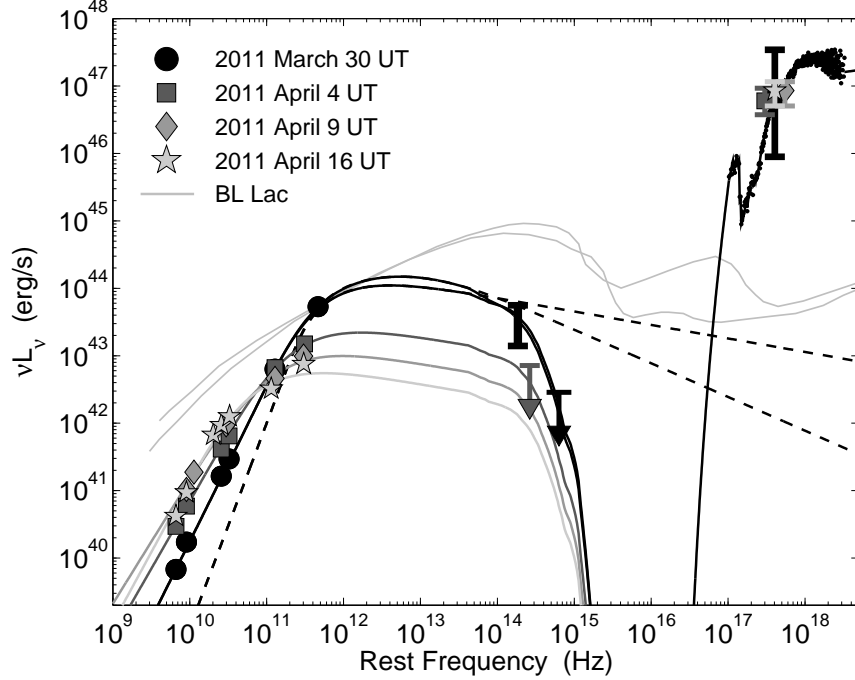


Figure 2. Spectral energy distributions (SEDs) of Swift J164449.3+573451 from radio to X-rays point to synchrotron emission from a relativistic outflow. Our radio observations cover decimeter to millimeter wavelengths at 5, 10, 15, and 22 d after the initial γ -ray detection. The NIR luminosity on March 30 can only be constrained within a factor of five due to the unknown contribution from the host galaxy; on April 4 the NIR upper limit is inferred from a *Hubble Space Telescope* image.⁶ Only an upper bound is available on the optical luminosity (black triangle) due to the lack⁶ of variable emission. The flux in the soft X-ray band is highly variable on March 30, but is more quiescent at 10, 15, and 22 d (extrema marked by vertical bars and mean brightness by solid symbols with points at 10 and 15 d shifted slightly in frequency for clarity). The radio, NIR, and optical data are well modeled by an evolving synchrotron spectrum (solid lines) with a large rest-frame optical extinction of $A_V > 3$ mag. The synchrotron curves for the March 30 SED are for two values of the synchrotron cooling frequency: $\nu_c \sim 2 \times 10^{13}$ Hz (steeper optically thin slope) and $\nu_c > 2 \times 10^{18}$ Hz (shallower optically thin slope). This model cannot explain the large X-ray luminosity, which remains nearly constant while the radio spectrum is evolving strongly. A representative model for the X-ray spectrum (data=black dots; model=black line) includes power-law ($F_\nu \propto \nu^{0.9}$) and blackbody ($kT \sim 1$ keV) components with significant absorption ($N_H \sim 2 \times 10^{22}$ cm⁻²), in agreement with the large optical extinction. Shown for comparison is the SED of the canonical blazar BL Lac in two separate states (varying in peak frequency and flux of the synchrotron component), normalized to the luminosity of Swift J164449.3+573451 at 345 GHz. The blazar SED provides a poor match.

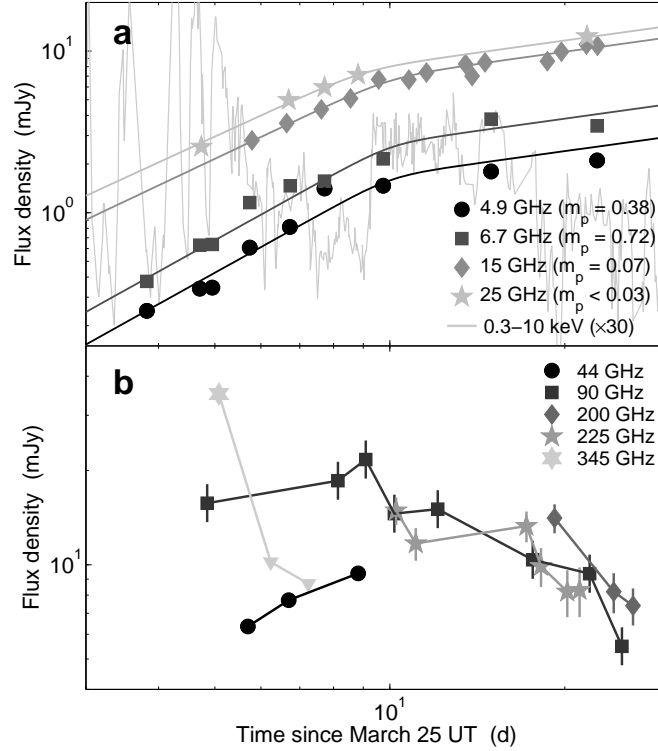


Figure 3. Radio light curves of Swift J164449.3+573451 at 5 – 345 GHz reveal interstellar scintillation. (a) Light curves at 5 – 25 GHz (error bars are smaller than symbols; see SI). These data are from the EVLA, the AMI Large Array, and the OVRO 40-m telescope. The lines are broken power law fits to the 5 – 25 GHz light curves, using March 25 as the initial time. The low frequency light curves exhibit significant interstellar scintillation, with the strongest modulation at 6.7 GHz. To calculate the expected interstellar scintillation we use the NE2001 Galactic Free Electron Density Model.¹² For the line of sight to Swift J164449.3+573451 ($l = 86.7111$, $b = 39.4415$) the scattering measure is $2.2 \times 10^{-4} \text{ kpc m}^{-20/3}$. With a scattering screen distance of 1 kpc the transition from weak to strong scattering occurs¹¹ at $\nu_0 \approx 10 \text{ GHz}$, while the Fresnel scale is $\theta_{F,0} \approx 1 \mu\text{as}$ (sizes are given as radii). At frequencies above ν_0 the modulation index is given by $m_p \approx (\nu/\nu_0)^{-17/12} (\theta_s/\theta_{F,0})^{-7/6}$. For frequencies below ν_0 refractive scintillation leads to $m_p \approx (\nu/\nu_0)^{17/30} (\theta_s/\theta_r)^{-7/6}$, where the refractive scale is $\theta_r = \theta_{F,0}(\nu/\nu_0)^{-11/5}$. Comparing these results to the observed modulation we infer a size of $\theta_s \approx 5 \mu\text{as}$. Also shown is the *Swift* X-ray light curve⁴ binned on a timescale of 15 min and multiplied by a factor of 1.3×10^{10} to fit on the same flux density scale as the radio data. The strong X-ray variability during the first 10 d is not accompanied by similar order of magnitude fluctuations in the radio bands, pointing to a distinct origin for the radio and X-ray emission. (b) Light curves at 44 – 345 GHz from the EVLA, CARMA, and the SMA (error bars are one standard deviation). These frequencies are mainly in the decline phase and therefore provide information on the peak of the synchrotron spectrum (Figure 2). Upper limits at 345 GHz are marked by triangles.

SUPPLEMENTARY INFORMATION

1 Archival Radio Non-detections of Swift J164449.3+573451

We inspected the location of Swift J164449.3+573451 in archival 1.4 GHz images from the NRAO VLA Sky Survey (NVSS) taken in March 1995, and the Faint Images of the Radio Sky at Twenty-cm (FIRST) survey taken in July 1998. No counterpart is detected to 3σ limits of about 1.5 mJy and 0.45 mJy, respectively. The non-detections place an upper bound on the radio luminosity of 6×10^{30} erg s⁻¹ Hz⁻¹ (March 1995) and 2×10^{30} erg s⁻¹ Hz⁻¹ (July 1998), thereby ruling out radio-loud AGN activity (typically $\lesssim 10^{33}$ erg s⁻¹ Hz⁻¹).

2 Expanded Very Large Array Observations

We observed Swift J164449.3+573451 with the EVLA beginning 0.82 d after the γ -ray trigger (see Table 1). We used the EVLA's new Wideband Interferometric Digital Architecture (WIDAR) correlator to obtain up to 2 GHz of bandwidth at several frequencies. At all frequencies, we used 3C286 for bandpass and flux calibration. Absolute flux calibration is accurate to $\sim 10\%$. At 1.4 GHz, we used J1634+6245 for phase calibration. For phase calibration at all other frequencies, we used J1638+5720 and also included a third calibrator, J1639+5357, at 5.8 GHz. Polarization calibration was not performed. The data were reduced and imaged with the Astronomical Image Processing System (AIPS) software package.

3 AMI Large Array observations

We observed with 6 antennas of the AMI Large Array (Mullard Radio Astronomy Observatory, Cambridge, UK) at 15.4 GHz with a bandwidth of 3.75 GHz beginning 2.79 d after the γ -ray trigger (see Table 1). The maximum baseline is about 110 m and the angular resolution is 25 arcsec. Observations ranged in duration from 45 min to 11 hr. Observations of the compact source J1638+5720 were interleaved at intervals of 10 m as a phase reference, and the flux density scale was established by regular observations of the calibrators 3C48 and 3C286. Absolute flux calibration is accurate to better than 10%. The

AMI array uses linearly-polarized feeds and measures Stokes I+Q. It does not measure any other combination of Stokes parameters. Polarization calibration is not reported here.

4 Owens Valley Radio Observatory 40-m Observations

We observed Swift J164449.3+573451 with the OVRO 40-meter telescope at a frequency of 15 GHz beginning 2.82 d after the γ -ray trigger (see Table 1). The 40-m telescope is equipped with a dual-beam Dicke-switched receiver with two symmetric, off-axis beams (each 2.5 arcmin full-width at half-maximum) separated azimuthally by 12.95 arcmin. The receiver has a 2.5 GHz noise-equivalent reception bandwidth. We used sky switching, alternating the source between the two beams to reduce atmospheric and ground pickup, and to account for the non-identical nature of the two beams. See Ref. 23 for further details of the telescope and receiver system. The flux scale is derived from observations of 3C286 using standard spectral models and coefficients²⁴ with an absolute uncertainty of 5%.

We note that daytime measurements of Swift J164449.3+573451 lead to consistently discrepant flux densities, most likely due to increased thermal emission from the ground. These discrepant measurements, as quoted in an initial GCN circular, have been used elsewhere⁵ to argue for a short variability timescale in the radio emission, and hence a large Lorentz factor of $\Gamma \gtrsim 10$. We do not support this conclusion, and indeed, as we show in Section 9, $\Gamma \gtrsim 10$ appears to lead to a non-self consistent model.

5 Combined Array for Research in Millimeter Astronomy Observations

We observed Swift J164449.3+573451 with CARMA beginning 1.85 d after the γ -ray trigger (see Table 1). CARMA is a heterogeneous array comprised of nine 6.1-m antennas and six 10.4-m antennas. Observations were taken at a rest frequency of 87.3 and 93.6 GHz with a total bandwidth ranging between 6.8 and 7.8 GHz. We used Neptune as our primary flux calibrator, and J1824+568 and J1638+573 as bandpass and phase calibrators, respectively. The overall uncertainty in the absolute flux calibration is 15%. Data calibration and imaging were done with the MIRIAD software package.

6 Submillimeter Array Observations

We observed Swift J164449.3+573451 with the Submillimeter Array (SMA; Ref. 25) beginning 0.28 d after the burst, followed by monitoring at 1.3 mm and 0.9 mm (see Table 1). Observations were made using at least seven of the eight antennas, in a wide range of weather conditions, with τ_{225} ranging from 0.04 to 0.3. For each observation, the full 8 GHz (4 GHz in each sideband separated by 10 GHz) were combined to increase the signal-to-noise ratio. The data were calibrated using the MIR software package developed at Caltech and modified for the SMA, while for imaging and analysis we used MIRIAD. Gain calibration was performed using J1642+689, 3C345, and J1849+670. Absolute flux calibration was performed using real-time measurements of the system temperatures, with observations of Neptune to set the scale, accurate to within 10 %. Bandpass calibration was done using 3C454.3, J1924-292, and 3C279.

7 Very Long Baseline Array Observations

We observed Swift J164449.3+573451 with the NRAO Very Long Baseline Array (VLBA) and the 100 m Effelsberg telescopes starting on 2011 April 2.25 UT for a duration of 7 hr at 8.4 and 22 GHz. The observations were performed with eight frequency bands of 8 MHz bandwidth each in dual circular polarization, resulting in a total data rate of 512 Mbps. We used J1638+5720, located only 0.92° from Swift J164449.3+573451, as a phase-referencing source at both frequencies. At 22 GHz, sources were switched every 40 seconds, while at 8.4 GHz we spent 40 seconds on the calibrator and 90 seconds on target. A second calibrator, J1657+5705, was also observed for six minutes at each frequency to check the calibration of the data. We also employed^{26,27} 30 min of geodetic blocks at the start and end of the observations for atmospheric calibration.

The data were correlated at the VLBA Array Operations Center in Socorro, New Mexico, and calibrated²⁸ using AIPS and ParselTongue. We applied the latest values of the Earth’s orientation parameters, and performed zenith delay corrections based on the results of the geodetic block observations. Total electron content maps of the ionosphere were used to correct for ionospheric phase changes. Amplitude calibration used system temperature measurements and standard gain curves. We performed “manual phase-calibration” using the data from one scan of J1638+5720 to remove instrumental phase offsets among the frequency bands. We then fringe fitted the data from J1638+5720.

Since J1638+5720 shows extended structure, we performed phase self-calibration first, and then amplitude and phase self-calibration to construct robust models at both frequencies. The calibration was transferred to the target source and J1657+5705. Residual phase calibration errors were removed by performing one round of phase self-calibration on the target with a solution interval of 30 min. The data were imaged in AIPS using robust weighting (ROBUST=0).

The 8.4 GHz images were restored with a beam of 1.03×0.46 mas at a position angle of 29° . We achieved a noise level of 30 Jy beam^{-1} , which is close to the expected thermal noise limit. Swift J164449.3+573451 was detected with a flux density of $1.71 \pm 0.03 \text{ mJy beam}^{-1}$. The 22 GHz images were restored with a beam of 0.44×0.24 mas at a position angle of 2° . We achieved a noise level of 120 Jy beam^{-1} , which is twice the expected thermal noise limit. Swift J164449.3+573451 was detected with a flux density of $4.68 \pm 0.12 \text{ mJy beam}^{-1}$. Absolute flux calibration is $\sim 15\text{-}20\%$.

The position of the source at both frequencies was measured from the purely phased referenced image (without phase self-calibration on the target). The formal uncertainties of the positions are $\sim 3 \times 8$ mas. The true uncertainty is dominated by systematic errors induced from residual atmospheric effects and an opacity effect (“core shift”) in the calibrator source. The position difference between the two frequencies is 61 mas in right ascension and 33 mas in declination. The absolute position as determined from the 22 GHz image is $\alpha_{\text{J2000}} = 16^{\text{h}}44^{\text{m}}49.93130^{\text{s}}$, $\delta_{\text{J2000}} = +57^\circ 34' 59.6893''$ with an uncertainty of 0.1 mas (68% confidence level) in each coordinate.

The limit of 0.25 mas corresponds to $r < 2 \times 10^{18}$ cm. This places an upper bound on the Lorentz factor of $\Gamma < 15$ (for relativistic expansion with $r \lesssim \Gamma^2 ct$ and a start time of 2011 March 25). Alternatively, we can use the inferred Lorentz factor of $\Gamma \sim 2$ to place an upper bound on the lifetime of the source of < 1.5 yr.

8 Optical Spectroscopy

We obtained two spectra of the host galaxy of Swift J164449.3+573451. The first spectrum was a 7200 s observation taken at a mean time of 2011 April 1.34 UT using Hectospec on the 6.5-m MMT and covered the observed wavelength range $3700 \text{--} 9150 \text{ \AA}$. The second one was taken in nod-and-shuffle mode using GMOS on the 8-m Gemini-North telescope

on 2011 April 4.62 UT (program GN-2011A-Q-4). The R400 grating was used to cover the wavelength range 4930–9180 Å.

The spectra are consistent with each other and exhibit the usual narrow emission lines of a star-forming galaxy ([OII] 3727, H β , [OIII] 4959–5007, H α) at a redshift of $z = 0.354$. Neither spectrum shows any evidence for a broad (FWHM ~ 1000 km s $^{-1}$) component to the H α line (SI Figure 1b), as would be seen in a Seyfert 1 galaxy (i.e., a galaxy with an unobscured actively-accreting central massive black hole). To examine the possibility that the host of Swift J164449.3+573451 contained a central black hole that was actively accreting prior to the current outburst, but which was obscured from our line of sight, we examined the ratios of several emission lines. Galaxies whose emission lines are powered by the ionizing radiation field of young stars can be separated from those powered by the harder radiation field produced by accretion onto a massive black hole using an excitation diagram²⁹ (SI Figure 1a). The host galaxy of Swift J164449.3+573451 is clearly located in the portion of the diagram associated with star-forming galaxies and not AGN. A small systematic uncertainty results from our inability to adequately correct for the underlying stellar absorption features with the signal-to-noise ratio of our current spectra, but that effect will only move the point associated with Swift J164449.3+573451 down and to the left, closer to the main locus of star-forming galaxies. In addition, neither of our spectra show any evidence for emission from high-excitation lines such as [NeV] 3345–3425, which would be evidence for an AGN. In summary, the spectra of the host galaxy of Swift J164449.3+573451 are consistent with expectations for a galaxy whose central black hole was not actively accreting prior to the current outburst.

9 Synchrotron Model of the Radio Emission

We assume that the radiation observed from Swift J164449.3+573451 in the radio band corresponds to synchrotron emission from relativistic electrons in a spherically expanding source. We use as inputs the observations at $\Delta t \sim 5, 10, 15,$ and 22 d (see Figure 2 of the main text). Given the shape of the spectrum we use $\alpha \sim -p$ in all three epochs.

We use the methods described in §3 of Ref. 30 to analyze each epoch independently. Although that work deals with gamma-ray bursts, which are highly relativistic, the basic framework is quite general. We describe the source by means of five parameters: the source radius, r , the bulk Lorentz factor, Γ , the Lorentz factor of the relativistic electrons that

produce the radiation at the synchrotron peak, ν_e (in the source frame), the number of relativistic electrons, N_e , and the magnetic field strength B (in the source frame). To determine these five parameters, we need five constraints. Three of these are provided by the measured values of ν_p , $F_{\nu,p}$, and ν_a , coupled with equations 1, 2, and 15 in Ref. 30.

A fourth condition is obtained by the assumption that the magnetic field and the relativistic particles are in equipartition. We write this condition as (see equations 33 and 34 Ref. 30):

$$E_B = B^2 r^3 / 2 = 10 E_e = 10 N_e m_e \Gamma c^2 \quad (1)$$

where the factor of 10 assumes that the total thermal energy in both electrons and protons is 10 times that in electrons alone.

Finally, for the fifth condition, we require the radius of the source to be consistent with ballistic expansion from the moment of the initial burst. The observed time of $\Delta t = 5$ d corresponds to a time of 3.7 d in the frame. Due to relativistic time compression, the actual time that the source would have expanded is $(3.7 \text{ d}) / (1 - \beta)$, where $\beta = v/c$ is the relativistic bulk expansion velocity of the source. Thus, the assumption of ballistic motion requires:

$$r = (3.7 \text{ d}) c / (1 - \beta) \quad (2)$$

Using the above five conditions, we obtain solution for the relevant parameters of the source at all four epochs. These solutions are summarized in Table 2. We find that all four epochs lead to the same expansion velocity of $\Gamma \approx 1.2$ (i.e., no deceleration) and an energy of $E_B = 10 E_e \approx 1.6 \times 10^{50}$ erg. The outflow mass, $8 \times 10^{-5} M_\odot$, combined with the constant expansion velocity, indicate that the density of the swept-up medium is $< 3 \times 10^3 \text{ cm}^{-3}$.

Fitting a linear trend to the expanding source size (as indicated by the data), we can estimate the initial formation date of the relativistic outflow (Figure 2). We find that this date is 2011 March 23–26 UT, in excellent agreement with the initial *Swift* detection of γ -ray emission on 2011 March 25 UT. This indicates that the formation of the relativistic outflow indeed coincided with the initial accretion episode onto the supermassive black hole.

Using the model, we have computed the synchrotron self-Compton (SSC) emission and find that the peak occurs at ≈ 0.1 keV and the luminosity at the peak is $\approx 2 \times 10^{45} \text{ erg s}^{-1}$. These values do not agree with the observed X-ray spectrum which peaks beyond 1 keV and

has a peak luminosity of $\sim 10^{47}$ erg s⁻¹ (observer frame). Thus, the model developed here suggests that the X-rays must arise either from a process other than SSC (e.g., Compton scattering of external radiation) or from a different region of the source.

Interestingly, in the framework of this model relativistic expansion with $\Gamma > 10$, as seen in most blazars, is ruled out. For $\Gamma > 10$, the radius r required to fit the observed radio flux and spectrum is much smaller than the radius implied by ballistic dynamics. It may be possible to avoid this difficulty by modeling the source as a highly collimated jet. However, the collimation angle of the jet would need to be much smaller than $1/\Gamma$, which is unlikely to be true. Another approach is to give up the condition of energy equipartition.

UT Date	Δt	Facility		F_ν	
	(d)		(GHz)	(mJy)	
Mar 31.28	2.74	EVLA	1.4	< 0 30	
Apr 1.28	3.74	EVLA	1.4	< 0 18	
Mar 31.28	2.74	EVLA	1.8	< 0 15	
Apr 1.28	3.74	EVLA	1.8	< 0 15	
Mar 29.36	0.82	EVLA	4.9	0 25	0 01
Mar 30.25	1.71	EVLA	4.9	0 34	0 02
Mar 30.49	1.95	EVLA	4.9	0 34	0 02
Mar 31.28	2.74	EVLA	4.9	0 61	0 02
Apr 1.27	3.73	EVLA	4.9	0 82	0 02
Apr 2.26	4.72	EVLA	4.9	1 48	0 02
Apr 4.28	6.74	EVLA	4.9	1 47	0 02
Apr 9.47	11.93	EVLA	4.9	1 80	0 03
Apr 17.27	19.73	EVLA	4.9	2 11	0 01
Mar 29.36	0.82	EVLA	6.7	0 38	0 01
Mar 30.25	1.71	EVLA	6.7	0 63	0 02
Mar 30.49	1.95	EVLA	6.7	0 64	0 02
Mar 31.28	2.74	EVLA	6.7	1 16	0 02
Apr 1.27	3.73	EVLA	6.7	1 47	0 02
Apr 2.26	4.72	EVLA	6.7	1 50	0 02
Apr 4.28	6.74	EVLA	6.7	2 15	0 02
Apr 9.47	11.93	EVLA	6.7	3 79	0 03
Apr 17.27	19.73	EVLA	6.7	3 44	0 01
Apr 9.46	11.92	EVLA	8.4	5 49	0 09
Mar 31.33	2.79	AMI-LA	15.0	2 80	0 45
Apr 1.18	3.65	AMI-LA	15.0	3 58	0 23
Apr 2.16	4.62	AMI-LA	15.0	4 35	0 28
Apr 3.10	5.56	AMI-LA	15.0	5 10	0 36
Apr 4.10	6.56	AMI-LA	15.0	6 67	0 51
Apr 5.33	7.79	AMI-LA	15.0	6 65	0 48
Apr 6.10	8.56	AMI-LA	15.0	7 36	0 45

Apr 8.03	10.49	AMI-LA	15.0	8 30	0 24
Apr 8.39	10.85	AMI-LA	15.0	7 01	0 13
Apr 9.12	11.58	AMI-LA	15.0	8 50	0 32
Apr 13.20	15.66	AMI-LA	15.0	8 66	0 40
Apr 14.27	16.73	AMI-LA	15.0	9 91	0 63
Apr 16.33	18.79	AMI-LA	15.0	10 96	0 89
Apr 17.30	19.76	AMI-LA	15.0	10 78	0 77
Mar 31.37	2.82	OVRO40	15.0	2 36	1 14
Apr 1.34	3.80	OVRO40	15.0	3 17	1 17
Apr 8.36	10.82	OVRO40	15.0	8 06	0 95
Apr 10.36	12.82	OVRO40	15.0	7 65	0 90
Apr 12.33	14.79	OVRO40	15.0	7 45	0 80
Apr 12.41	14.87	OVRO40	15.0	6 60	1 22
Apr 15.35	17.81	OVRO40	15.0	10 54	0 93
Apr 19.33	21.79	OVRO40	15.0	11 99	1 03
Apr 21.36	23.82	OVRO40	15.0	9 55	1 04
Mar 30.24	1.70	EVLA	19.1	2 12	0 02
Apr 1.24	3.70	EVLA	19.1	4 36	0 05
Apr 2.26	4.72	EVLA	19.1	5 25	0 03
Apr 3.36	5.82	EVLA	19.1	6 38	0 05
Apr 4.27	6.73	EVLA	19.1	5 31	0 03
Apr 16.38	18.84	EVLA	19.1	12 01	0 03
Mar 30.24	1.70	EVLA	24.4	3 01	0 03
Apr 1.24	3.70	EVLA	24.4	5 58	0 06
Apr 2.26	4.72	EVLA	24.4	6 70	0 03
Apr 3.36	5.82	EVLA	24.4	7 88	0 12
Apr 4.27	6.73	EVLA	24.4	6 60	0 03
Apr 16.38	18.84	EVLA	24.4	12 69	0 03
Mar 31.28	2.70	EVLA	44	6 35	0 10
Apr 1.24	3.70	EVLA	44	7 71	0 08
Apr 3.36	5.82	EVLA	44	9 38	0 08
Apr 2.68	5.14	CARMA	87	18 6	0 3

Apr 3.63	6.09	CARMA	87	21 ζ	0 2
Apr 4.72	7.18	CARMA	87	14 ζ	0 4
Apr 6.63	9.09	CARMA	87	15 ζ	0 2
Apr 12.15	14.61	CARMA	87	10 ζ	0 2
Apr 16.60	19.06	CARMA	87	9 3 ζ	0 5
Apr 19.61	22.07	CARMA	87	5 4 ζ	0 3
Mar 30.39	1.85	CARMA	94	15 ζ	0 3
Apr 16.60	19.06	CARMA	94	10 ζ	1 0
Apr 13.66	16.12	SMA	200	14 ζ	1 5
Apr 18.70	21.16	SMA	200	8 ζ	1 2
Apr 20.74	23.20	SMA	200	7 ζ	1 0
Mar 28.82	0.28	SMA	225	< 33	
Apr 4.74	7.20	SMA	225	14 ζ	1 5
Apr 5.40	7.86	SMA	225	11 ζ	0 4
Apr 11.63	14.10	SMA	225	13 ζ	1 5
Apr 12.66	15.12	SMA	225	9 ζ	1 4
Apr 14.65	17.11	SMA	225	8 ζ	1 4
Apr 15.67	18.13	SMA	225	8 ζ	2 2
Mar 30.39	1.85	SMA	345	35 ζ	1 0
Mar 31.39	1.85	SMA	345	< 10	2
Apr 1.71	4.17	SMA	345	< 8	7

Table 1: Radio observations of Swift J164449.3+573451. All values of Δt are relative to the γ -ray trigger. For times relative to the initial detection (2011 March 25 UT) as used in the main text add 3.54 d. Flux measurement errors are one standard deviation systematic errors. Absolute flux scaling depends on the instrument. See SI text for details.

Table 2: Summary of Radio SED Modeling

Parameter	$\Delta t = 5$ d	$\Delta t = 10$ d	$\Delta t = 15$ d	$\Delta t = 22$ d
ν_p (GHz; rest-frame)	600	250	140	80
$F_{\nu,p}$ (mJy; rest-frame)	80	40	30	25
r (10^{16} cm)	1.0	1.7	2.6	4.7
Γ	1.2	1.2	1.1	1.2
β	0.5	0.5	0.5	0.5
n_e	150	140	140	140
B (G)	17	8	4.6	2.6
N_e (10^{53})	1.0	1.1	1.5	2.6
n_e (10^4 cm $^{-3}$)	2.4	0.5	0.2	0.06
$E_B = 10E_e$ (10^{50} erg)	1.4	1.5	1.9	2.9
θ_s (as)	0.6	1.0	1.5	2.6

Table 2: Summary of relativistic model results for the four broad-band SEDs shown in Figure 2 of the main text. The top portion lists the observed synchrotron parameters, while the bottom portion lists the model fit results.

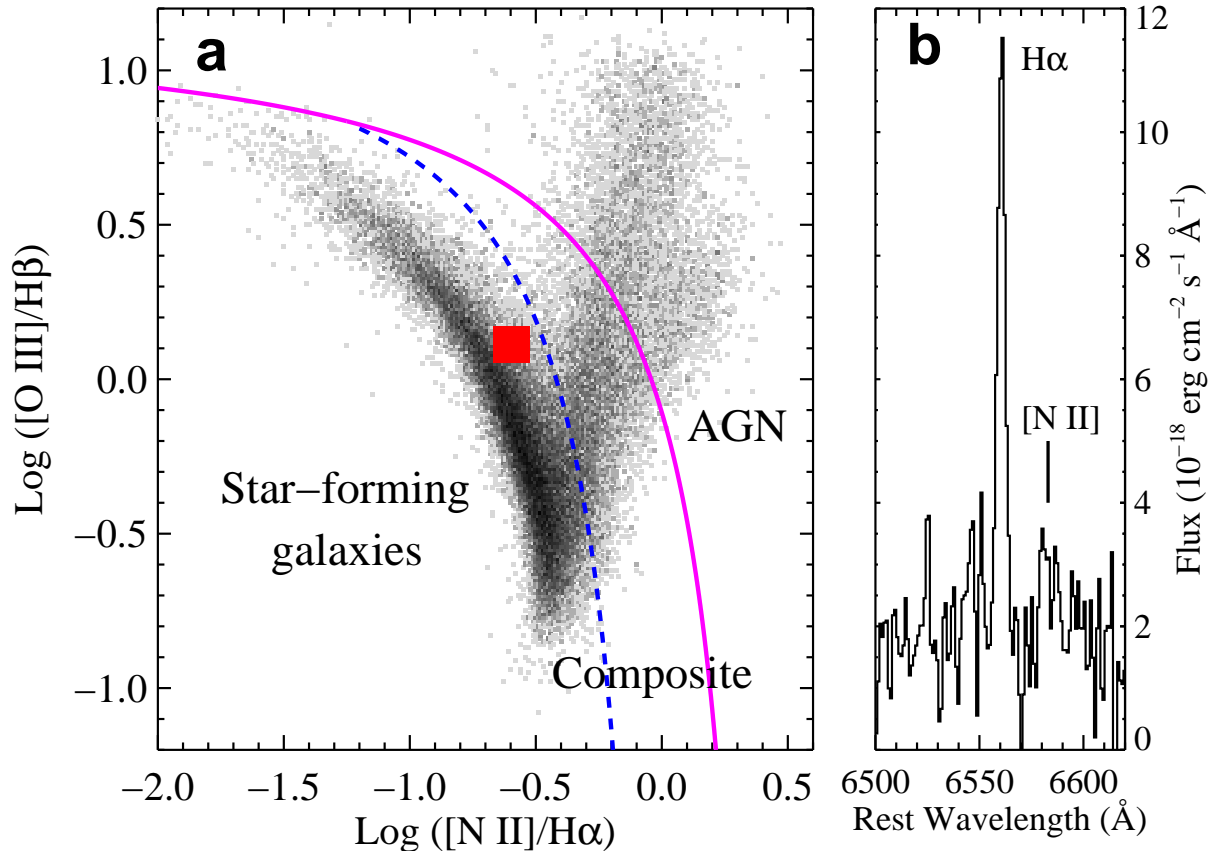


Figure 1. Optical spectroscopy of the host galaxy of Swift J164449.3+573451 shows no indication of AGN activity. (a) Excitation diagram comparing the observed line ratios of the host galaxy of Swift J164449.3+573451 to a sub-sample of galaxies observed^{31,32} in the Sloan Digital Sky Survey. The emission lines in objects found to the right of the magenta line are powered by accretion onto massive black holes, while those between the blue dashed line and the solid magenta line show³³ “composite” spectra of star formation plus AGN activity. Objects to the left of both lines have emission lines dominated³³ by star formation activity. The host galaxy (red square) is clearly in the portion of the diagram associated with star-forming galaxies. (b) The region around the $\text{H}\alpha$ line in the Gemini spectrum. No broad component is observed as would be expected for an active Seyfert 1 galaxy.

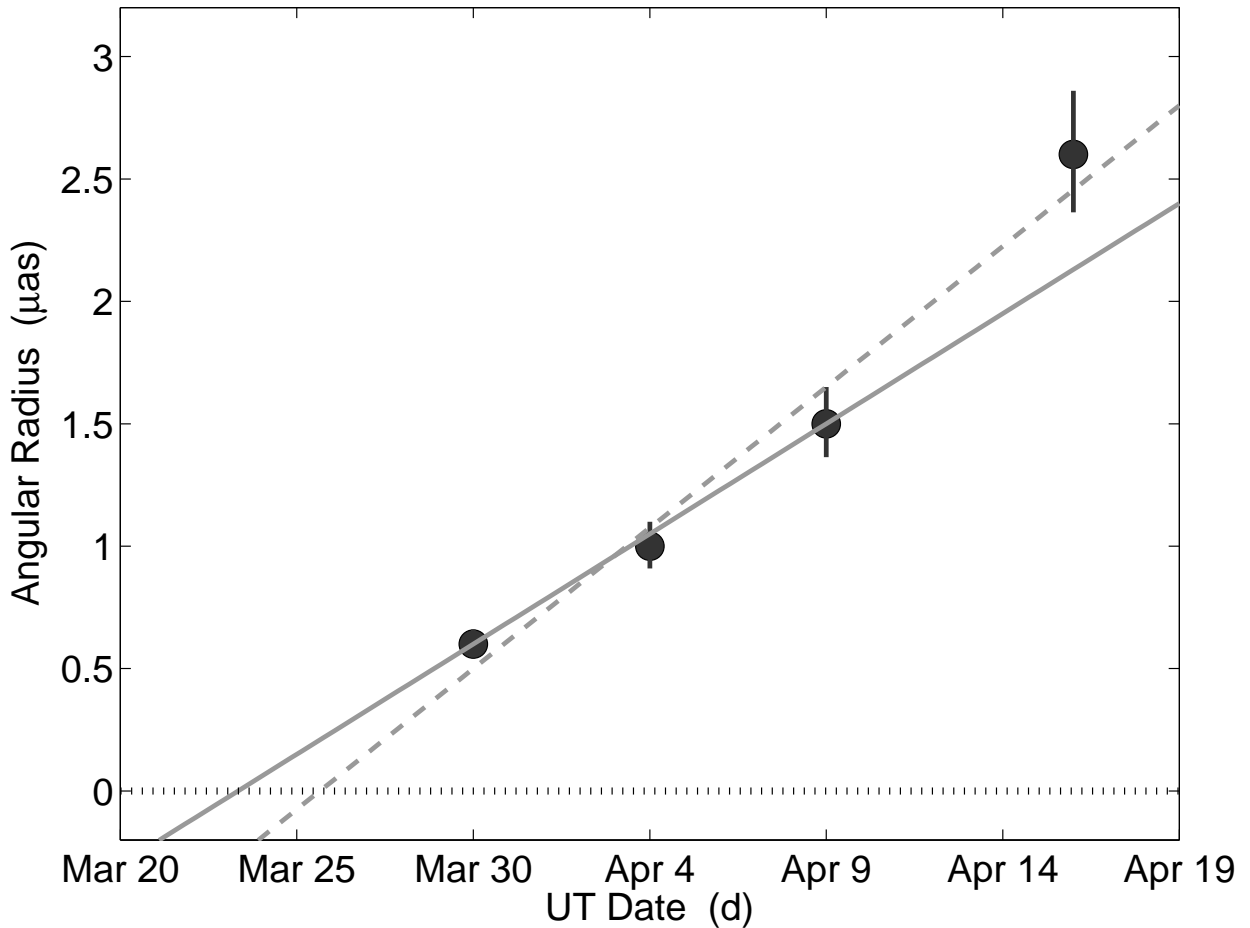


Figure 2. The radius of the radio emitting region inferred from the relativistic model indicates a formation date in excellent agreement with the initial burst. Angular radius of the radio emitting region as a function of UT date. The linear growth in source size indicates a formation date of 2011 March 23-26 UT, in agreement with the initial *Swift* detection of γ -ray emission on 2011 March 25 UT. The solid and dashed lines indicate fits to the first three epochs and all four epochs, respectively. We note that the last epoch on 2011 April 16 UT has a larger uncertainty than the preceding measurements.

-
22. Miller, L., Peacock, J. A. & Mead, A. R. G. The bimodal radio luminosity function of quasars. *Mon. Not. R. Astr. Soc.* **244**, 207–213 (1990).
 23. Richards, J. L., Max-Moerbeck, W., Pavlidou, V., King, O. G. *et al.* Blazars in the *Fermi* Era: The OVRO 40-m Telescope Monitoring Program. *ArXiv:1011.3111* (2011).
 24. Baars, J. W. M., Genzel, R., Pauliny-Toth, I. I. K., & Witzel, A. The Absolute Spectrum of Cas A - An Accurate Flux Density Scale and a Set of Secondary Calibrators. *Astron. Astrophys.* **61**, 99–106 (1977).
 25. Ho, P. T. P., Moran, J. M. & Lo, K. Y. The Submillimeter Array. *Astrophys. J.* **616**, L1–L6 (2004).
 26. Brunthaler, A., Reid, M. J. & Falcke, H. in *Future Directions in High Resolution Astronomy* (ed J. Romney & M. Reid) 455 (2005).
 27. Reid, M. J., Menten, K. M., Brunthaler, A., Zheng, X. W., Moscadelli, L. *et al.* Trigonometric Parallaxes of Massive Star-Forming Regions. I. S 252 & G232.6+1.0. *Astrophys. J.* **693**, 397–405 (2009).
 28. Kettenis, M., van Langevelde, H. J., Reynolds, C. & Cotton, B. in *Astronomical Data Analysis Software and Systems XV* (ed C. Gabriel, C. Arviset, D. Ponz, & S. Enrique) 497 (2006).
 29. Baldwin, J. A., Phillips, M. M. & Terlevich, R. Classification parameters for the emission-line spectra of extragalactic objects. *Publ. Astr. Soc. Pacific* **93**, 5–19 (1981).
 30. Kumar, P. & Narayan, R. GRB 080319B: evidence for relativistic turbulence, not internal shocks. *Mon. Not. R. Astr. Soc.* **395**, 472–489 (2009).
 31. Kauffmann, G., Heckman, T. M., Tremonti, C., Brinchmann, J., Charlot, S. *et al.* The host galaxies of active galactic nuclei. *Mon. Not. R. Astr. Soc.* **346**, 1055–1077 (2003).
 32. Tremonti, C. A., Heckman, T. M., Kauffmann, G., Brinchmann, J., Charlot, S. *et al.* The Origin of the Mass-Metallicity Relation: Insights from 53,000 Star-forming Galaxies in the Sloan Digital Sky Survey. *Astrophys. J.* **613**, 898–913 (2004).
 33. Kewley, L. J., Groves, B., Kauffmann, G. & Heckman, T. The host galaxies and classification of active galactic nuclei. *Mon. Not. R. Astr. Soc.* **372**, 961–976 (2006).
-